Asymptotic solution of transonic nozzle flows with homogeneous condensation. I. Subcritical flows

Can F. Delale, Günter H. Schnerr, and Jürgen Zierep

Citation: Physics of Fluids A: Fluid Dynamics **5**, 2969 (1993);
View online: https://doi.org/10.1063/1.858704
View Table of Contents: http://aip.scitation.org/toc/pfa/5/11
Published by the American Institute of Physics

Asymptotic solution of transonic nozzle flows with homogeneous condensation. I. Subcritical flows

Can F. Delale[a),b)] Günter H. Schnerr, and Jürgen Zierep
Institut für Strömungslehre und Strömungsmaschinen, Universität (TH) Karlsruhe, Germany

(Received 3 August 1992; accepted 7 June 1993)

The one-dimensional (1-D) asymptotic solution of subcritical transonic nozzle flows with nonequilibrium homogeneous condensation is presented. An algorithm based on a local iterative scheme that exhibits the asymptotic solution in distinct condensation zones is developed for transonic moist air expansions under atmospheric supply conditions. Two models that characterize the state of the condensed phase as water drops or ice crystals are employed, together with the classical nucleation theory and Hertz–Knudsen droplet growth law. It is shown that the 1-D asymptotic predictions are in good agreement with the recent static pressure measurements of moist air expansions in relatively slender nozzles when the condensed phase is assumed to consist purely of water drops.

I. INTRODUCTION

Nonequilibrium condensation in transonic nozzle flows has been investigated both experimentally and theoretically for a long period, not only because it has application in various technologies such as steam turbine technology, but also that it can be used to improve our understanding of condensation kinetics. It is commonly viewed as a process attributed to the collapse of the supersaturated vapor state (onset of condensation) initiated by homogeneous nucleation reaching a state of thermodynamic equilibrium in a few microseconds by subsequent violent droplet growth in the supersonic region. During this process a considerable amount of heat is released, causing the pressure, temperature, and density of the working fluid to continuously rise over a relatively small thickness (subcritical flow). If the amount of heat exceeds a certain value, normal shock waves occur due to compressive effects from excessive heat release, and the flow in this case is termed supercritical. This event was first reported by Prandtl[1] and the problem was later formulated by Oswatitsch.[2] Presently the subject can be studied in the informative articles by Wegener and Mack,[3] Stever,[4] Wegener,[5] Hill,[6] Barschdorff,[7] Gyarmathy,[8] and in their extensive references. Qualitative description of the condensation zones with detailed analytical structure is also available in Blythe and Shih[9] and Clarke and Delale[10] using asymptotic methods. Actually, asymptotic methods serve as alternatives against which computational results can be compared. They offer analytical structure of the flow field so that physically distinct condensation zones can be compared with measurements mapped over the same regions.

In this paper we present the asymptotic solution of transonic nozzle flows in distinct condensation zones in a format convenient for numerical predictions. For this reason the integroalgebraic formulation of the flow and state equations is considered. The asymptotic analysis of the condensation rate equation incorporating the contribution from initial critical nuclei is carried out quite generally in terms of some thermodynamic functions and parameters that enter the nucleation rate equation and the radius-independent droplet growth rate law. These thermodynamic functions and parameters are identified from the classical nucleation theory and the Hertz–Knudsen droplet growth law for transonic moist air expansions under atmospheric supply conditions by assuming two distinct models for the condensed phase. An algorithm based on an iterative scheme is presented for the predictions of the asymptotic solution for such flows. The effect of wall curvature is then exhibited by employing two distinct nozzles, one slender and the other effectively two dimensional, but with the same cooling rate. It is shown that the predictions of the asymptotic theory for transonic moist air expansions in slender nozzles under atmospheric supply conditions agree well with experiments when the condensed phase is assumed to consist purely of water drops. In nozzles of relatively large wall curvature the predictions show the necessity of extending the asymptotic solution to account for the 2-D flow field structures in various condensation zones.

Only predictions of subcritical transonic nozzle flows of moist air under atmospheric supply conditions are presented in this paper.

II. FLOW AND RATE EQUATIONS IN CONDENSING NOZZLE FLOWS

We consider the quasi-one-dimensional transonic nozzle flow of a mixture of a condensible vapor and a carrier gas with initial specific humidity ω_0, initial relative humidity φ_0, and initial temperature T_0, and assume that the state of the condensible vapor crosses the coexistence line during its expansion. In this and all subsequent sections we use subscript 0 to denote the initial reservoir conditions and subscript s to denote saturation conditions. Using the

[a)]Alexander von Humboldt Fellow.
[b)]Permanent address: Department of Mathematics, Bilkent University, Ankara, Turkey.

 0899-8213/93/5(11)/2969/13/$6.00

normalization carried out in Blythe and Shih[9] and Clarke and Delale,[10] the flow equations and the thermal equation of state of the mixture of perfect gases can be conveniently written as

$$\rho u A = u_s, \tag{1}$$

$$pA + \rho u^2 A = 1 + u_s^2 + R(g,x), \tag{2}$$

$$c_{p0}T + \tfrac{1}{2}u^2 - L(T)g = c_{p0} + \tfrac{1}{2}u_s^2 = c_{p0}T_0, \tag{3}$$

$$p = \rho T(1 - H^{-1}g), \tag{4}$$

where

$$R(g,x) = \int_{x_s}^{x} p\frac{dA}{d\xi}d\xi, \tag{5}$$

and where the conventional momentum differential equation is replaced by the integral momentum theorem, Eq. (2). In Eqs. (1)–(5) ρ, p, and T are, respectively, the density, the pressure, and the temperature of the mixture, $c_{p0} \equiv \gamma/(\gamma-1)$ denotes the dimensionless specific heat of the mixture at constant pressure, $L(T)$ is the latent heat of condensation at the local temperature T, u is the flow speed, A is the local cross-sectional area of the nozzle, and g is the normalized condensate mass fraction. All the flow variables, except u, are normalized with respect to saturation conditions, so that $\rho_s = p_s = T_s = L_s = 1$. The cross-sectional area A is normalized with respect to its value at saturation and the axial coordinate x is normalized with respect to the nozzle throat height ($2y^*$). The flow speed u and the condensate mass fraction g are normalized somewhat differently by

$$g \equiv \frac{\mu_0}{\mu_v} H g' \tag{6}$$

and

$$u \equiv \frac{u'}{\sqrt{\Re T_s'/\mu_0}}, \tag{7}$$

where μ_0 and μ_v are, respectively, the mixture molecular weight in the reservoir and the vapor molecular weight, $\Re = 8.314$ J/mol K is the universal gas constant, g' is the actual condensate mass fraction, u' is the actual flow speed, T_s' is the actual saturation temperature, and $H \equiv (\mu_v L_s')/(\Re T_s')$ is a suitable normalization constant with L_s', denoting the actual latent heat of condensation at saturation (in this work all primed variables denote the actual flow variables).

The system of Eqs. (1)–(4) can be solved for the flow speed u in functional form as

$$u(g,x) = \frac{[1 + u_s^2 + R(g,x)]/(2u_s) \pm \sqrt{\Delta(g,x)}}{[\gamma + 1 + (\gamma-1)H^{-1}g]/(2\gamma)}, \tag{8}$$

where $\Delta(g,x)$ is defined by

$$\Delta(g,x) = \left(\frac{1 + u_s^2 + R(g,x)}{2u_s}\right)^2 - \left(\frac{\gamma + 1 + (\gamma-1)H^{-1}g}{2\gamma}\right) \times (1 - H^{-1}g)\left(T_0 + \frac{gL(T)}{c_{p0}}\right). \tag{9}$$

In Eq. (8), the $(-)$ sign should be chosen for the subsonic branch and the $(+)$ sign for the supersonic branch of the flow field. The remaining flow variables ρ, p, and T can then be given in functional form in terms of $u(g,x)$ as

$$\rho(g,x) = \frac{u_s}{u(g,x)A(x)}, \tag{10}$$

$$p(g,x) = \frac{1 + u_s^2 + R(g,x) - u_s u(g,x)}{A(x)}, \tag{11}$$

$$T(g,x) = T_0 + \frac{L(T)g}{c_{p0}} - \frac{[u(g,x)]^2}{2c_{p0}}. \tag{12}$$

The above functional relations (8)–(12) will presumably yield a complete solution when the condensate mass fraction g is solved from the corresponding rate equation. The nonequilibrium condensation rate equation for g is constructed[2,9,10] from a condensation nuclei production rate J, conveniently normalized as

$$J = \Sigma(p_v,T)\exp[-K^{-1}B(p_v,T)], \tag{13}$$

and a normalized droplet growth rate law, assumed to be independent of the droplet radius,

$$\frac{dr}{dx} = \lambda\Omega(p_v,T,g). \tag{14}$$

Here $\Sigma(p_v,T)$ is a normalized multiplicative factor in the rate equation, $B(p_v,T)$ is the normalized activation function, K is the nucleation parameter, assumed small ($K \ll 1$), $\Omega(p_v,T,g)$ is a conveniently normalized droplet growth function, and λ is the droplet growth parameter, assumed large ($\lambda \gg 1$). Furthermore, the droplet radius r is normalized with respect to a conveniently defined droplet normalization radius [e.g., see Delale[11] or Eq. (34) of this paper] and p_v, the normalized vapor pressure, is related to the mixture pressure p by

$$p_v = \frac{\mu_0\omega_0 H - \mu_v g}{\mu_0\omega_0(H-g)}p. \tag{15}$$

Assuming that the normalized critical radius for nuclei formation at any location x is $r^*(x)$, the integral condensation rate equation takes the form (Oswatitsch,[2] Blythe and Shih,[9] and Clarke and Delale[10])

$$g(x) = \int_{x_s}^{x}\left(r^*(\xi) + \lambda\int_{\xi}^{x}\Omega(\eta)d\eta\right)^3\Sigma(\xi)A(\xi) \times \exp[-K^{-1}B(\xi)]d\xi, \tag{16}$$

where it is understood that the values assumed by the thermodynamic functions r^*, Σ, B, and Ω at any location along the nozzle axis are evaluated from the local thermodynamic state utilizing Eq. (15). The integral condensation rate equation (16) is strongly coupled to the flow relations

(8)–(12), so that, although they form a closed system, Eqs. (8)–(12), together with Eqs. (5) and (16), do not seem to constitute an explicit solution. However, the rate equation contains two disparate parameters: $K(\ll 1)$, the nucleation parameter signifying a large nucleation time; and $\lambda(\gg 1)$, the droplet growth parameter signifying a small droplet growth time. This suggests asymptotic analysis of the rate equation in the double limit as $K\to 0$ and $\lambda\to\infty$.

III. ASYMPTOTIC SOLUTION OF THE RATE EQUATION AND CONDENSATION ZONES

Asymptotic analysis of the condensation rate equation (16) with different ordering of the double limit as $K\to 0$ and $\lambda\to\infty$ has already been carried out in Blythe and Shih[9] and Clarke and Delale,[10] where the initial critical radius r^* of nuclei formation is neglected. For numerical predictions, the contribution to the normalized condensation rate equation from the normalized initial critical radius r^* may become very important, especially near the onset of condensation, where the nucleation rate is near its peak; therefore, it is essential to improve the asymptotic theories by taking into account the initial critical radius correction. Moreover, the previous asymptotic theories[9,10] demand the ordering of the double limit as $K\to 0$ and $\lambda\to\infty$, so that the onset of condensation and the order of magnitudes of the flow variables in different condensation zones can be determined. In particular, determining the order of magnitude estimates of the flow variables at the onset (which depends on the ordering of the double limit as $K\to 0$ and $\lambda\to\infty$) is very essential in each theory, since the perturbation expansions and the scaling coordinates in the proceeding zones depend on these estimates. Different ordering of the double limit leads to different perturbation expansions of the flow variables and thus to different scaling coordinates in the condensation zones following onset. Furthermore, the perturbation solutions of the flow variables given in each asymptotic theory[9,10] for the condensation zones following onset neglect the contribution from area change, and thus cannot, in general, secure a reliable physical solution in these zones. The above-mentioned difficulties of the previous asymptotic theories have to be overcome before any numerical predictions can be made.

In what follows, aside from justifying the convenience of the scaling variables of Eqs. (D3) and (D4) introduced in Appendix D, solely for numerical predictions, no use of the ordering of the double limit as $K\to 0$ and $\lambda\to\infty$ will be made; therefore, the asymptotic expressions given in the appendices of this paper should be regarded as being quite general. The asymptotic analysis of the condensation rate equation of this paper is indeed carried out in a unique fashion. Moreover, the perturbation solution of the various asymptotic theories[9,10] in the condensation zones following onset is replaced by a local iterative solution, which converges to the actual solution. We let x_l denote the turning point of the normalized activation function B, i.e., the point where the nucleation rate is at its maximum. This turning point will be referred to as the "relative onset point." The asymptotic analysis then distinguishes different regions, which may be divided into physically distinct condensation zones, according to their locations with respect to this relative onset point x_l. A typical variation of the normalized activation function B along the nozzle axis exhibiting the various physically distinct condensation zones is shown in Fig. 1(a).

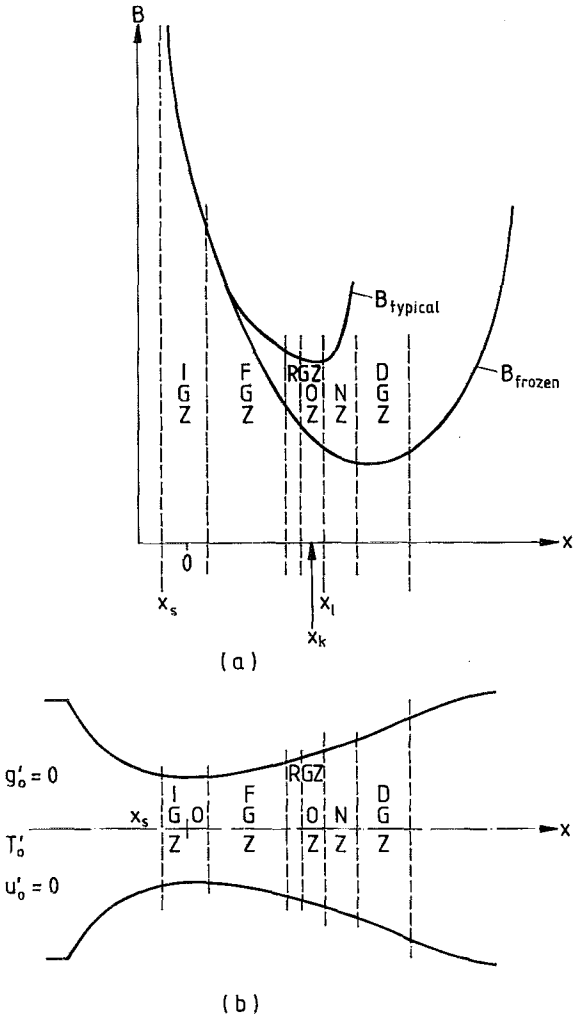

FIG. 1. (a) Typical and frozen behavior of the normalized activation function B in transonic nozzle flows (x_s is the saturation point, x_k is the empirically or numerically defined onset point, and x_l is the relative onset point, where the nucleation rate is maximum). (b) Characteristic condensation zones in transonic nozzle flows.

In the interval $x_s\leqslant x\leqslant x_l$ the flow is nearly frozen, i.e.,

$$R(g,x)\approx R_f(x)\equiv\int_{x_s}^{x}p_f(\xi)\frac{dA}{d\xi}d\xi \tag{17}$$

and

$$L(T)\approx L(T_f), \tag{18}$$

where by subscript f we denote the condensate-free frozen flow for which $g\equiv 0$. In particular, $R_f(x)$ can be evaluated exactly from Eq. (17) as

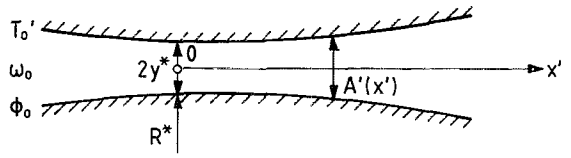

FIG. 2. Geometry of nozzles employed.

$$R_f(x)=\frac{M_s}{M_f(x)}\sqrt{\frac{1+[(\gamma-1)/2]M_s^2}{1+[(\gamma-1)/2]M_f^2(x)}}\times[1+\gamma M_f^2(x)]-\gamma M_s^2-1, \tag{19}$$

where $M_f(x)$ is the condensate-free frozen Mach number distribution and M_s is its value at saturation. In this approximation the flow functionals $u(g,x)$, $\rho(g,x)$, etc., of Eqs. (8)–(12), consequently the thermodynamic functions B, Σ, Ω, and r^* become known functions of g and x, i.e.,

$$u=\tilde{u}(g,x), \quad \rho=\tilde{\rho}(g,x), \text{ etc.,} \tag{20}$$

and

$$B=\tilde{B}(g,x), \quad \Sigma=\tilde{\Sigma}(g,x), \quad \text{etc.} \tag{21}$$

Thus, in the interval $x_s \leqslant x \leqslant x_l$ the rate equation (16) can be completely decoupled from the flow and state equations and becomes a nonlinear Volterra integral equation for $g(x)$. The variation of the normalized activation function B, as shown in Fig. 1, then discriminates the various physically distinct condensation zones using Laplace's method[12–14] in the double limit as $K\to 0$ and $\lambda\to\infty$.

In the initial growth (IGZ) and further growth (FGZ) zones, $dB/dx=O(1)$ by definition. The initial growth zone (IGZ) is defined as the zone where the number of condensation nuclei or clusters of critical size, created in the parent phase by highly improbable collisions of the vapor molecules (homogeneous nucleation), is not sufficient enough to influence the isentropic flow field. Thus the flow remains frozen (isentropic) throughout this zone and all of the flow variables and thermodynamic functions assume their frozen values (i.e., $p=p_f$, $\rho=\rho_f$, $T=T_f$, $B=B_f$, $\Omega=\Omega_f$, etc.). In the further growth zone (FGZ), B starts to deviate from B_f (although this deviation may be negligibly small in some cases), and as a result dB/dx and dB_f/dx [both of $O(1)$ in this zone] become numerically distinct. In spite of the fact that the condensation nuclei production rate continuously increases throughout this zone, this rate is not sufficient for the onset of condensation to occur in this zone for smooth flows (if the onset of condensation occurs in this zone, meaning that a sufficient number of condensation nuclei for onset becomes available in this zone, then the flow cannot be continuous or subcritical since there would then be an abrupt change in the sign of dB/dx from excessive latent heat addition giving rise to a normal shock wave). The two zones IGZ and FGZ distinguished above physically are not asymptotically distinct and the asymptotic solution of the rate equation (16) presented in Appendix A applies to both zones, although it can further be simplified in IGZ (see Appendix A). Consequently, the asymptotic solutions in these zones (in the nearly frozen approximation) are now directly obtained from the asymptotic solution of the rate equation presented in Appendix A, together with the functional relations (8)–(12).

As dB/dx diminishes to $O(K^{1/2})$ as $K\to 0$, the solution given above in FGZ is no longer valid, and we are, by definition, in the rapid growth (RGZ) and onset (OZ) zones. Actually, the onset zone can be thought as being embedded in RGZ. It contains the "onset point" x_k, which is defined empirically (e.g., by static pressure measurements) or numerically (e.g., by fixing a certain value for g as an onset value for a given working fluid with similar supply conditions and nozzle geometry), that marks the beginning of the collapse of the supersaturated vapor state. In particular, the nucleation rate peaks at the relative onset point x_l, which is defined by $(dB/dx)_{x=x_l}=0$ and that marks the end of the onset zone. Once again these two zones are not asymptotically distinct, and the asymptotic solution of the rate equation (16) presented in Appendix B applies to both zones. This asymptotic solution, together with the functional relations (8)–(12) and the nearly frozen approximations (17) and (18), determine the flow field inside these zones (in the nearly frozen approximation), together with the relative onset point x_l.

The asymptotic solutions presented above in the interval $x_s \leqslant x \leqslant x_l$ for the condensation zones IGZ, FGZ, RGZ, and OZ utilize the nearly frozen approximation given by Eqs. (17) and (18). The actual flow field in these zones can, in principle, be calculated from the functional relations (8)–(12) and the asymptotic solutions of Appendices A and B by iteration, starting with the nearly frozen flow field; however, this is not necessary since it can be shown[10] that the deviation of the actual flow field from its nearly frozen approximation in these zones can be neglected for any practical consideration.

For $x \geqslant x_l$ we have two physically and asymptotically distinct condensation zones: The nucleation zone with growth (NZ) and the droplet growth zone (DGZ), as shown in Fig. 1. The nucleation zone with growth NZ proceeds the onset zone OZ and ends as the nucleation rate diminishes. In this zone, where both nucleation and droplet growth are important, the nucleation rate decreases ($dB/dx>0$) until it completely diminishes. Droplet growth on condensation nuclei of size exceeding the critical size results in considerable heat release to the flow. As a result an increase in the pressure, temperature, and density and a decrease in the flow speed of the mixture are first observed in this zone. The asymptotic solution of the rate equation (16) presented in Appendix C, together with the functional relations (8)–(12) and Eq. (5), determine the local flow field inside this zone. Downstream of NZ, where nucleation has completely ceased for any practical consideration, droplet growth takes over and we are, by definition, in the droplet growth zone (DGZ). In this zone a remarkable amount of latent heat (supposedly not exceeding a critical amount for smooth flows) is set free, giving rise to an increase in the temperature, pressure, and density of the mixture over a relatively small thickness (this phe-

nomenon is inappropriately called a "condensation shock" in the literature). The approach to saturated thermodynamic equilibrium of the two-phase mixture also takes place in this zone. The asymptotic solution presented in Appendix D, together with Eqs. (8)–(12) and Eq. (5), form a complete system that determines the local flow field in DGZ. It should also be mentioned that the solution for NZ and DGZ of this work is quite different from that given in Clarke and Delale, since in this format of solution there is no more need to carry out the flow field perturbation expansions, which in the first approximation neglect the contribution from the area variation in these zones. The asymptotic analysis presented in this section completely determines the local flow field with detailed structure in distinct condensation zones in terms of the thermodynamic functions r^*, B, Σ, and Ω and the parameters K and λ underlying the physics of nonequilibrium condensation. Identification of these thermodynamic functions and parameters requires a detailed discussion of the phenomenology of nonequilibrium condensation.

IV. KINETICS OF CONDENSATION

The kinetics of nonequilibrium condensation can be studied in two stages: The initial new phase formation in the form of condensation nuclei, called nucleation, and the subsequent growth of these nuclei into small drops or crystals, called droplet growth. Small drops or crystals may be formed in the presence of inert impurities (heterogeneous nucleation or condensation) or by statistical cluster formation due to thermal fluctuations (homogeneous nucleation or condensation). Condensation in nozzle flows usually implies a homogeneous nucleation mechanism; therefore, we will herein only consider homogeneous condensation. The first attempt on the mechanism of spontaneous formation of condensation nuclei in metastable vapors was taken by Volmer and Weber[15] by application of Boltzmann's distribution law for the equilibrium cluster distribution of condensation nuclei of critical size and the theory was further improved by Farkas,[16] Becker and Döring,[17] Volmer,[18] Zeldovich,[19] and Frenkel[20] (today this theory is known as the classical nucleation theory). The more recent statistical mechanical theories that take into account the translational, rotational, and vibrational contributions from clusters have been suggested by Lothe and Pound,[21] Courtney,[22] and can also be found in Zettlemoyer.[23] A comprehensive discussion of various nucleation theories is given in the work of Skripov[24] and Feder *et al.*[25] A recent improvement on the classical nucleation theory is also available from the work of Dillmann and Meier,[26] who employ a semiphenomenological model for the formation energy of condensation nuclei. Despite all, no universally accepted theory of nucleation exists yet. Even when some of the poorly known thermodynamic functions that enter the theories are treated as curve-fitted parameters, some theories work better for some fluids, whereas they yield poorer results for other fluids in comparison with existing experimental data. For nozzle experiments with moist air to be considered herein, it has been demonstrated over years that the classical nucleation theory yields better results; therefore, we proceed with the application of the classical nucleation theory. In this theory the rate of condensation nuclei production J' per unit time and per unit volume is given by (e.g., see Wegener[5])

$$J'=\sqrt{\frac{2}{\pi}}\sigma'\frac{\rho_v'^2}{\rho_{\mathrm{con}}'}(m')^{-3/2}\exp\left(-\frac{\Delta G^*}{kT'}\right), \tag{22}$$

where m' is the mass of a single vapor molecule, ρ_v' and ρ_{con}' are, respectively, the actual vapor density and the actual density of the condensed phase, $k=1.38\times10^{-23}$ J/K is Boltzmann's constant, σ' is the surface tension, which, in general, depends on the actual temperature T' and on the droplet size (characterized by the actual droplet radius r', assuming all condensation nuclei to be spherical in shape), and ΔG^* is the Gibbs formation energy for a nucleus of critical size given by

$$\Delta G^*=\tfrac{4}{3}\pi(r'^*)^2\sigma', \tag{23}$$

with the critical radius r'^* to be evaluated from the Thomson–Gibbs equation,

$$r'^*=\frac{2\sigma'}{\rho_{\mathrm{con}}'R_vT'\,\mathrm{Ln}\,S}. \tag{24}$$

In Eq. (24), $R_v\equiv\Re/\mu_v=k/m'$ denotes the gas constant of the vapor and $S\equiv p_v'/p_{s,\infty}'(T')$ denotes the supersaturation ratio, where $p_{s,\infty}'(T')$ is the actual planar saturation pressure at T'. Having determined the production rate of condensation nuclei of critical size in terms of the thermodynamic functions σ', ρ_{con}' and $p_{s,\infty}'$, which presumably will be supplied, we proceed to discuss the second stage of condensation kinetics, i.e., the growth of condensation nuclei of critical size.

In condensing nozzle flows droplet growth is dominated by further condensation of the vapor on the unstable nuclei (coagulation of growing drops or crystals can be neglected). The rate of vapor condensing on unstable nuclei is governed by the rate at which latent heat is carried away from the surface of the drop or crystal into the cooler vapor. The heat and mass transfer mechanisms, which assume no slip and infinite vapor surrounding, are described either by continuum or molecular laws, depending on the Knudsen number Kn defined by

$$\mathrm{Kn}\equiv\frac{l'}{2r'},$$

where l' is the mean-free path of the vapor molecules. For moist air expansions to be considered in this study, where $\mathrm{Kn}\gg1$, it is well known that the classical Hertz–Knudsen droplet growth law for free molecular flows, which, for steady one-dimensional flow, assumes the form

$$u'\frac{dr'}{dx'}=\alpha(T')\frac{p_{s,\infty}'(T')}{\rho_{\mathrm{con}}'\sqrt{2\pi R_vT'}}(S-1), \tag{25}$$

can be used. In Eq. (25) all primed variables denote actual variables, and $\alpha(T')$ is the condensation coefficient (sometimes known as the accommodation coefficient), defined as the ratio of molecules sticking to the drop or crystal to those impinging on it. A detailed derivation of Eq. (25)

from the kinetic theory of gases, together with the conventional assumptions made and the continuum droplet growth law, which will not be discussed herein, can be found in the informative studies of Hill,[6] Gyarmathy,[8] and their extensive references.

With the above discussed nucleation and droplet growth theories on hand, the identification of the normalized thermodynamic functions such as B, Σ, etc., and of the parameters λ and K still requires some knowledge of the thermodynamic properties, such as the latent heat L', the surface tension σ', the density of the condensed phase ρ'_{con}, the condensation coefficient α, and the planar saturation pressure $p'_{s,\infty}$ in the operational range of nozzle flows to be considered. In order to be able to obtain information on these thermodynamic properties, we restrict our discussion to transonic moist air expansions under atmospheric supply conditions. In this case the surface tension σ' can be taken to be independent of droplet size so that it can be set equal to its planar value σ'_∞ and ρ'_{con} can be approximated by its average value $\bar{\rho}_{\text{con}}$ ($\approx$920–1000 kg/m^3) over the operational temperature range of the nozzle. The required thermodynamic properties can then be determined from the following two models of the condensed phase.

(a) Liquid Model (LM). In this model we assume the condensed phase to consist purely of water droplets. For atmospheric supply conditions the planar saturation pressure can be evaluated from the expression given in Sonntag and Heinze[27] as

$$p'_{s,\infty}(T')=T'^{\nu_0}\exp\left(\nu_1+\nu_2T'+\nu_3T'^2+\frac{\nu_4}{T'}\right)(\text{N/m}^2),$$

where $\nu_0=2.4576$, $\nu_1=21.125$, $\nu_2=-2.7246\times10^{-2}$, $\nu_3=1.6853\times10^{-5}$, $\nu_4=-6.095\times10^3$, and where T' is measured in K. The expression for the latent heat can then be found by the Clausius–Clapeyron equation in the form

$$L'(T')=R_v(\nu_2T'^2+2\nu_3T'^3+\nu_0T'-\nu_4)\ \ (\text{kJ/kg}).$$

The planar surface tension in this model is calculated from the empirical relation,

$$\sigma'_\infty(T')=\begin{cases}[76.1+0.155(273.15-T')]\times10^{-3}\ \ (\text{N/m}),\\ \quad\text{for } T'\geqslant249.4\ \text{K},\\ [1.131-3.709\times10^{-3}T']T'^4\times10^{-10}\ \ (\text{N/m}),\\ \quad\text{for } T'<249.4\ \text{K},\end{cases}$$

suggested by Schnerr and Dohrmann,[28] fitted to the experimental data of Peters and Paikert,[29] and the condensation coefficient is taken from the empirical relation of Peters and Paikert[29] as

$$\alpha(T')=\begin{cases}0.5, & \text{for } T'>270\ \text{K},\\ 1-0.0125(T'-230), & \\ \quad\text{for } 230\ \text{K}\leqslant T'\leqslant270\ \text{K}, & \\ 1, & \text{for } T'<230\ \text{K}.\end{cases}$$

(b) Ice Model (IM). In this model the latent heat of condensation L' is taken from Sonntag and Heinze[27] as

$$L'=\begin{cases}2501\ (\text{kJ/kg}), & \text{for } T'\geqslant273.15\ \text{K},\\ 2839\ (\text{kJ/kg}), & \text{for } T'<273.15\ \text{K}.\end{cases}$$

The expression for the planar saturation pressure (e.g., see Sonntag and Heinze), in turn, can be evaluated from

$$p'_{s,\infty}=611\exp\left[\frac{L'}{R_v}\left(\frac{1}{273.15}-\frac{1}{T'}\right)\right]\ (\text{N/m}^2).$$

The planar surface tension in this model is extrapolated from Grigull[30] as

$$\sigma'_\infty(T')=\begin{cases}[75.75+0.151(273.15-T')]\times10^{-3}\ \ (\text{N/m}),\\ \quad\text{for } T'\geqslant273.15\ \text{K},\\ [96.0-0.29(273.15-T')]\times10^{-3}\ \ (\text{N/m}),\\ \quad\text{for } T'<273.15\ \text{K}.\end{cases}$$

Due to lack of reliable data, in this model the condensation coefficient will be treated as a curve fitting parameter ranging between 0.1 and 1.0.

A. Identification of thermodynamic functions and parameters

From the above discussion of condensation kinetics we are now in a position to identify the thermodynamic functions and parameters entering the asymptotic theory. Utilizing Eqs. (22)–(24), together with Eq. (5), the normalization of Sec. II and the information furnished above in the liquid and ice models, the nucleation rate equation can now be written in the form convenient for the asymptotic expressions given in the appendices, as

$$J'=\zeta'J=\zeta'\Sigma(p,T,g)\exp[-K^{-1}B(p,T,g)], \tag{26}$$

where

$$\zeta'\equiv\sqrt{\frac{2}{10^3\pi}\left(\frac{T'_0}{100}\right)^3\left(\frac{T'_s}{100}\right)}(m')^{-3/2}\frac{\omega_0^2\rho_s'^2}{\bar{\rho}_{\text{con}}}, \tag{27}$$

and where the thermodynamic functions B and Σ and the nucleation parameter K are identified by

$$B(p,T,g)\equiv[f(T)]^3[\text{Ln}\,S(p,T,g)]^{-2}, \tag{28}$$

$$\Sigma(p,T,g)\equiv\sqrt{\frac{f(T)}{T^3}}\left(\frac{\omega_0\mu_0H-\mu_vg}{\omega_0\mu_0(H-g)}\right)^2p^2 \tag{29}$$

and

$$K\equiv\frac{3.0\times10^{15}}{16\pi}k^3\left(\frac{\bar{\rho}_{\text{con}}}{m'}\right)^2\left(\frac{100}{T'_0}\right)^9, \tag{30}$$

with

$$S(p,T,g)\equiv\frac{p'_s}{T'^{B_1}_s}\frac{(\omega_0\mu_0H-\mu_vg)}{\mu_v(H-g)}\times\frac{p}{T^{B_1}\exp(A_0+A_1T+A_2T^2+B_0/T)}. \tag{31}$$

In Eqs. (28), (29), and (31) the function $f(T)$ and the coefficients A_0, A_1, A_2, B_0, and B_1 are to be evaluated from (a) in the liquid model (LM),

$$f(T)=\begin{cases}(100/T_s')(100/T_0')^3[76.1+0.155(273.15-T_s'T)]T^{-1}, & \text{for } T\geqslant 249.4\ \text{K}/T_s' \\ (T_s'/T_0')^3[11.34-0.037\,09T_s'T]T^3, & \text{for } T<249.4\ \text{K}/T_s',\end{cases} \tag{32}$$

and $A_0=21.125$, $A_1=-2.7246\times10^{-2}T_s'$, $A_2=1.6853\times10^{-5}T_s'^2$, $B_0=-6.095\times10^3/T_s'$, and $B_1=2.4576$; and (b) in the ice model (IM),

$$f(T)=\begin{cases}(100/T_s')(100/T_0')^3[75.75+0.151(273.15-T_s'T)]T^{-1}, & \text{for } T\geqslant 273.15\ \text{K}/T_s', \\ (100/T_s')(100/T_0')^3[96.0-0.29(273.15-T_s'T)]T^{-1}, & \text{for } T<273.15\ \text{K}/T_s',\end{cases} \tag{33}$$

and $A_0=6.415+[L'/(273.15\,R_v)]$, $A_1=A_2=B_1=0.0$, and $B_0=-L'/(R_vT_s')$, where L' takes on one of its constant values in this model.

In normalizing the droplet growth equation (25), i.e., in identifying the functions Ω and λ of Eq. (14), we first define the normalization radius r_d' of a droplet [which follows directly from the construction of the condensation rate equation (16), where the normalized radius is defined as $r\equiv r'/r_d'$] by

$$r_d'\equiv\left(\frac{3\mu_v\rho_s'u_s'}{8\pi\mu_0 Hy^*\zeta'\bar{\rho}_{\text{con}}}\right)^{1/3}. \tag{34}$$

Utilizing the normalization of Sec. II, together with Eqs. (3) and (15) and the above liquid and ice models of the condensed phase, the droplet growth rate equation (25) can be cast into the form of Eq. (14) by identifying Ω and λ as

$$\Omega(p,T,g)\equiv\alpha(T)\frac{10^{2(B_1-1)}T^{(B_1-0.5)}\exp(A_0+A_1T+A_2T^2+B_0/T)}{\sqrt{2c_{p0}(1-T)+2L(T)g+u_s^2}}[S(p,T,g)-1] \tag{35}$$

and

$$\lambda\equiv\left(\frac{T_s'}{100}\right)^{(B_1-1)}\frac{y^*}{\bar{\rho}_{\text{con}}\Re r_d'}\sqrt{\frac{2\mu_0\mu_v}{\pi}}, \tag{36}$$

where $S(p,T,g)$ is given by Eq. (31) and where $\alpha(T)$, together with the coefficients A_0, A_1, A_2, B_0, and B_1 are to be evaluated from the appropriate model (LM) or (IM), employed for the condensed phase. In a similar fashion, introducing the normalized critical radius by $r^*\equiv r'^*/r_d'$, the Thomson–Gibbs equation (24) yields

$$r^*(p,T,g)=\frac{2m'}{10^5r_d'\bar{\rho}_{\text{con}}k}\left(\frac{T_0'}{100}\right)^3\frac{f(T)}{\text{Ln}\,S(p,T,g)}, \tag{37}$$

where $f(T)$ once again is to be evaluated from the appropriate model (LM or IM) of the condensed phase.

Thus we have determined the thermodynamic functions B, Σ, Ω, and r^* [given by Eqs. (28), (29), (35), and (37), respectively], and the parameters K and λ [given by Eqs. (30) and (36), respectively] for use in the asymptotic solution of transonic moist air expansions in nozzles under atmospheric supply conditions. For other working fluids (e.g., pure steam, nitrogen, etc.) and under different supply conditions (e.g., high supply pressures), the identification of the above thermodynamic functions and parameters has to be reconsidered in a similar manner from the appropriate nucleation and droplet growth theories accompanied by the relevant thermodynamic properties of the working fluids. In such a case care should be taken in identifying the parameters K and λ, so that the thermodynamic functions $f(T)$ and $\Omega(p,T,g)$ remain of $O(1)$ numerically, and as in Eq. (30), K depends only on initial reservoir conditions and, on the condensible component of the working fluid, whereas, as in Eq. (36), λ, in addition, depends on the nozzle geometry, on the carrier gas, and on the nature of the condensed phase (liquid or crystalline phase).

V. PREDICTIONS OF ASYMPTOTIC THEORY

In this section we discuss the predictions of the asymptotic theory for transonic moist air expansions under atmospheric supply conditions. We first present an algorithm for computing the flow field of condensing moist air expansions in nozzles by the asymptotic theory, bringing together the results of Secs. III and IV. This algorithm naturally begins with the computation of the classical frozen solution for condensate-free expansion of the air–steam mixture, from which the condensate-free frozen Mach number distribution $M_f(x)$ can be determined. Using this solution one identifies the saturation point x_s as the point where the relative humidity φ_0 (or the supersaturation S) reaches unity during the expansion. All the flow variables can then be normalized appropriately in reference to the saturation conditions, as discussed in Sec. II. Moreover, since only subcritical flows are considered in this paper (a detailed treatment of supercritical flows is given in the companion paper), in Eq. (8), the condition $\Delta(g,x)\geqslant 0$ for all x is taken for granted, and for the sign in front of the square root it is understood that the $(-)$ sign is chosen in the subsonic and the $(+)$ sign in the supersonic regions of the flow field.

For nearly frozen flows valid in the interval $x_s\leqslant x\leqslant x_l$, the frozen impulse function $R_f(x)$ is to be evaluated exactly by Eq. (19), and the latent heat L is to be approximated by the local frozen temperature dependence, as given by Eq. (18). In IGZ and FGZ the value of the condensate mass fraction g is presumably to be solved from Eqs. (A1)–(A3) of Appendix A using, respectively, Eqs. (28), (29), (35), and (37) for B, Σ, Ω, and r^* and Eqs.

(30) and (36) for the parameters K and λ. The derivatives $\partial\tilde{B}/\partial g$ and $\partial\tilde{B}/\partial x$ that enter Eq. (A3) of Appendix A are to be evaluated by applying the chain rule for differentiation to Eq. (28) and by simultaneously utilizing Eqs. (8)–(12). The local solution $g(x)$ is then determined from Eqs. (A1)–(A3) of Appendix A, starting with the condensate-free frozen solution or with the nearby upstream solution by iteration. In these regions the solution for the local flow field at any x is then exactly given by Eqs. (8)–(12) by inserting the local solution $g(x)$ and by utilizing Eqs. (18) and (19), respectively, for L and $R(g,x)$. The same procedure applies in RGZ and OZ, where dB/dx, now evaluated from Eq. (A3) of Appendix A, diminishes to $O(K^{1/2})$ as $K\to 0$. In this case Eqs. (A1)–(A3) of Appendix A for IGZ and FGZ are to be replaced by Eqs. (B1)–(B10) of Appendix B. All of the first and second partial derivatives of the thermodynamic functions of Eqs. (B1)–(B10) of Appendix B should again be evaluated by application of the chain rule to Eqs. (28), (29), (35), and (37) that, respectively, identify B, Σ, Ω, and r^* and by utilizing the functional relations (11) and (12) for p and T. The local flow field at any x in RGZ and OZ is similarly obtained by inserting the local value $g(x)$ of the condensate mass fraction, obtained from the solution of Eqs. (B1)–(B10) of Appendix B, into the functional relations of Eqs. (8)–(12). Finally, the relative onset point x_l can be identified as the point where $dB/dx\equiv 0$ and all of the flow variables at this point can, in turn, be calculated.

In NZ and DGZ, where $x\geqslant x_l$, the procedure somewhat differs since in these regions the nearly frozen approximations of Eq. (18) for L and of Eq. (19) for $R(g,x)$ can no longer be employed. In this case, for use in the functional relations of Eqs. (8)–(12), $R(g,x)$ should be evaluated directly from the defining relation (5) by numerical integration using the upstream pressure distribution. The latent heat $L(T)$ can first be approximated by its most nearby upstream value at each location in these zones and can then be corrected for iteratively if and when desired. The system of Eqs. (C1)–(C5) of Appendix C and the functional relations (8)–(12) then yield an explicit solution for the local flow field at any x in NZ. In DGZ, where the nucleation rate given by Eq. (26) has diminished for all practical purposes, Eq. (D6) of Appendix D, together with the solution of the relaxation rate equation (D7), of Appendix D, which can be achieved by simple quadrature integration or by more sophisticated numerical methods (e.g., the Runga–Kutta method with predictor corrector), and the functional relations (8)–(12), yield the complete explicit solution for the local flow field. In this zone a saturated thermodynamic equilibrium state is finally achieved by nature of the relaxation rate equation (D7) of Appendix D.

The above algorithm for the asymptotic solution of transonic moist air expansions under atmospheric supply conditions is employed in two different nozzles whose geometric specifications are shown in Table I (see also Fig. 2). Nozzle 1 seems to fit better into the one-dimensional consideration for which better agreement of the 1-D asymptotic solution is reached, whereas nozzle 2 is effectively two

TABLE I. Geometric specifications of the circular arc nozzles used in Figs. 3–7.

Nozzle	Throat height $2y^*$ (mm)	Circular nozzle radius R^* (mm)	First employed by
Nozzle 1	30	400	Schnerr (1986)
Nozzle 2	60	200	Barschdorff (1967).

dimensional and is used to exhibit the effect of wall curvature on the flow field in various condensation zones. Along the axis of nozzle 1, the 1-D and 2-D adiabatic pressure distributions seem to agree well within an error, which can be neglected for all practical purposes. Figures 3–5 show the 1-D predictions of the asymptotic theory in the transonic expansion of moist air through nozzle 1 under spec-

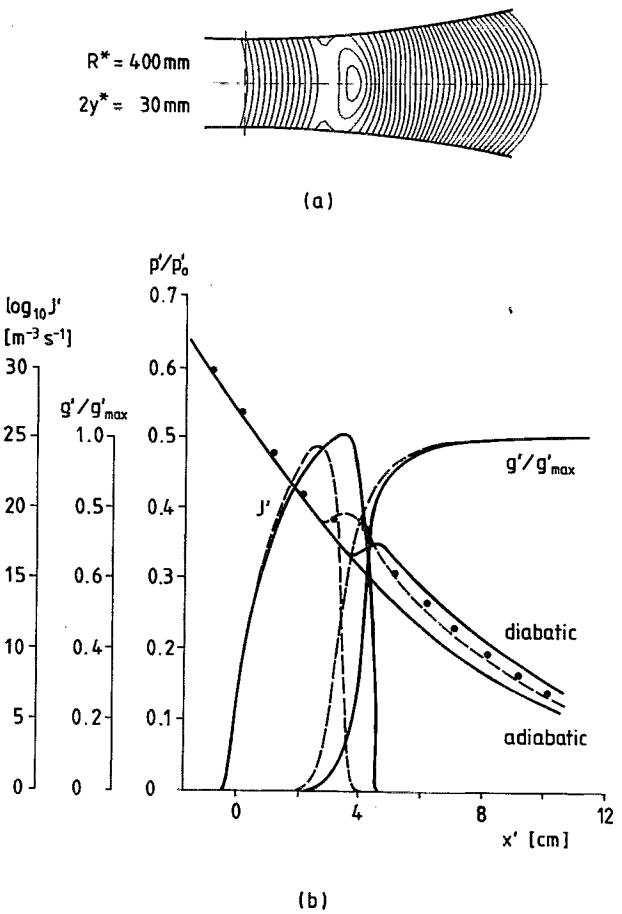

FIG. 3. (a) The Mach number ($M>1$) contours from the numerical 2-D simulation of Schnerr and Dohrmann (Ref. 28) in nozzle 1 under the atmospheric supply conditions $\varphi_0=36.4\%$, $\omega_0=6.6$ g/kg, and $T'_0=296.6$ K (the increment between any two successive contours is $\Delta M=0.02$). (b) Distribution of the pressure, the nucleation rate, and the condensate mass fraction along the axis of nozzle 1 under the atmospheric supply conditions $\varphi_0=36.4\%$, $\omega_0=6.6$ g/kg, and $T'_0=296.6$ K. ●, static pressure measurements in experiments conducted by Schnerr (Ref. 31); ---, numerical 2-D finite volume simulation in the ice model with $\alpha=0.2$ by Schnerr and Dohrmann (Ref. 28) ($T'_s=277.7$ K, $T'_k=226.4$ K, $\Delta T'_{ad}\equiv T'_s-T'_k=51.4$ K, $M_k=1.245$, $J'_{max}=0.22\times 10^{25}$ m^{-3} sec^{-1}); ——, 1-D asymptotic solution in the ice model for $\alpha=0.2$ ($T'_s=277.7$ K, $T'_k=215.2$ K, $\Delta T'_{ad}\equiv T'_s-T'_k=61.1$ K, $M_k=1.36$, $J'_{max}=0.12\times 10^{26}$ m^{-3} sec^{-1}, $K=0.893\times 10^{-2}$, and $\lambda=412.17$).

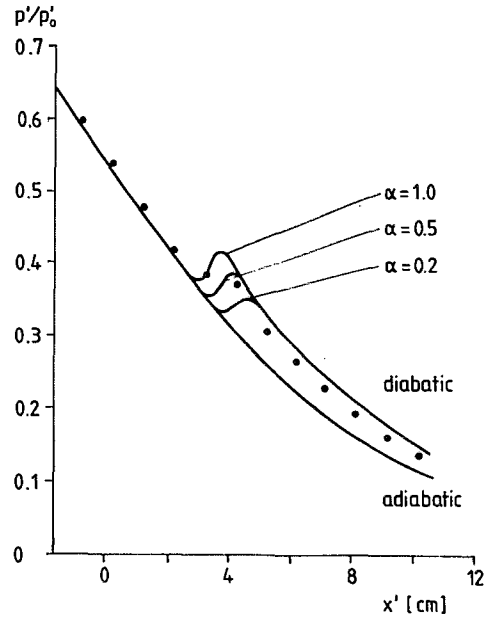

FIG. 4. The pressure distribution along the axis of nozzle 1 under the atmospheric supply conditions of Fig. 3. ●, experimental measurements by Schnerr (Ref. 31), ——, 1-D asymptotic solution by varying the condensation coefficient α in the ice model.

ified atmospheric supply conditions, in comparison with the 2-D numerical finite volume computations by Schnerr and Dohrmann[28] and the recent experiments conducted by Schnerr.[31] Figure 3(a) exhibits the Mach number contours (for $M>1$) in nozzle 1 from the 2-D numerical simulation of Schnerr and Dohrmann, which shows that the wall curvature effects are only important downstream of the condensation zones. Figure 3(b) shows the predictions of the asymptotic theory in the ice model with $\alpha=0.2$, in comparison with the 2-D numerical simulation of Schnerr and Dohrmann and the experiments conducted by Schnerr. In this case the predicted onset of condensation (defined by the point where $g'_k=0.2$ g/kg, the subscript k referring to onset conditions) in the asymptotic theory seems to be delayed within a few millimeters and the downstream pressures after saturated equilibrium is reached appear a few percent higher than the experimentally measured values. It is clearly seen here that the predictions of the asymptotic theory fit better to the experimental results when α is between 0.5 and 0.6, in contrast to the value $\alpha=0.2$ in the 2-D numerical simulation of Schnerr and Dohrmann. However, as demonstrated in Fig. 5 when the liquid model is employed for the predictions of the asymptotic theory, better agreement with experimental results is achieved. In this case the predicted pressure distribution downstream of the condensation zones is again a few percent higher than the measured one.

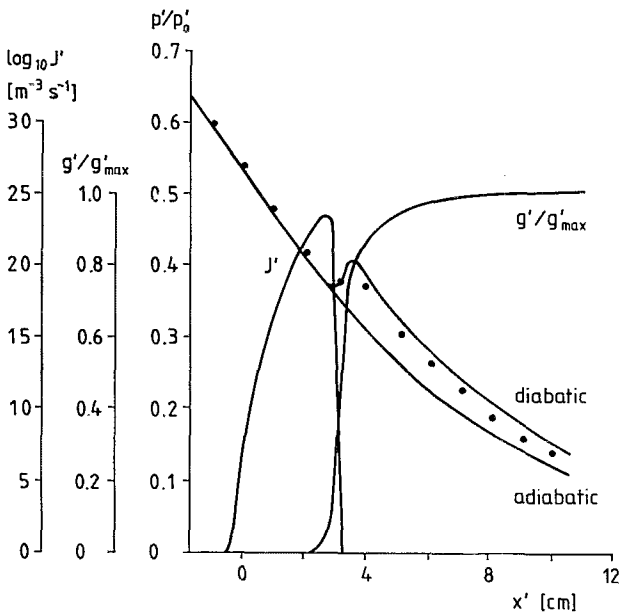

FIG. 5. Distribution of the pressure, the nucleation rate, and the condensate mass fraction along the axis of nozzle 1 under the atmospheric supply conditions $\varphi_0=36.4\%$, $\omega_0=6.6$ g/kg, $T'_0=296.6$ K. ●, static pressure measurements in experiments conducted by Schnerr (Ref. 31); ——, 1-D asymptotic solution in the liquid model, where $\alpha=1$ for $x>x_k$ ($T'_s=277.5$ K, $T'_k=222.16$ K, $\Delta T'_{ad}\equiv T'_s-T'_k=55.34$ K, $M_k=1.29$, $J'_{max}=0.47\times10^{24}$ m^{-3} sec^{-1}, $K=0.893\times10^{-2}$, and $\lambda=5024.3$).

Figures 6 and 7 show the predictions of the asymptotic theory in moist air expansions under specified atmospheric supply conditions through nozzle 2. The 2-D Mach number distribution of Fig. 6(a) from Schnerr and Dohrmann demonstrates the importance of the 2-D effects arising from the wall curvature of nozzle 2 during expansion. In this case the adiabatic pressure distributions in one dimension and two dimensional along the nozzle axis differ considerably. Figure 6(b) shows the pressure distribution of the 1-D asymptotic theory in the ice model with different values of α against that along the nozzle axis in the 2-D numerical simulation of Schnerr and Dohrmann employing the ice model with $\alpha=0.2$ and the experimental measurements by Schnerr. In this case, rather than agreement upstream of the condensation zones, downstream agreement by the asymptotic theory is achieved (e.g., for $\alpha=0.5$), which clearly demonstrates the necessity of the overall 2-D flow field computation. On the other hand, Fig. 7 shows the predictions of the asymptotic theory for moist air expansions through nozzle 2 in the liquid model, which seem to agree better than those in the ice model within the limitations of the 1-D theory.

The above results demonstrate that the predictions of the 1-D asymptotic theory in the liquid model are quite satisfactory when slender nozzles such as nozzle 1 are used, whereas the 1-D asymptotic theory needs to be modified to account for the wall curvature effects when effectively 2-D nozzles such as nozzle 2 are employed. Such a modification is, in principle, available only for Prandtl–Meyer flows, with nonequilibrium condensation from the work of Delale[11] and Clarke and Delale,[32] but it has to be reconsidered for the 2-D flow field computation in nozzles.

VI. DISCUSSION

Transonic nozzle flows of moist air under atmospheric supply conditions are investigated by the asymptotic solution of the condensation rate equation constructed from the classical nucleation rate equation and the Hertz–

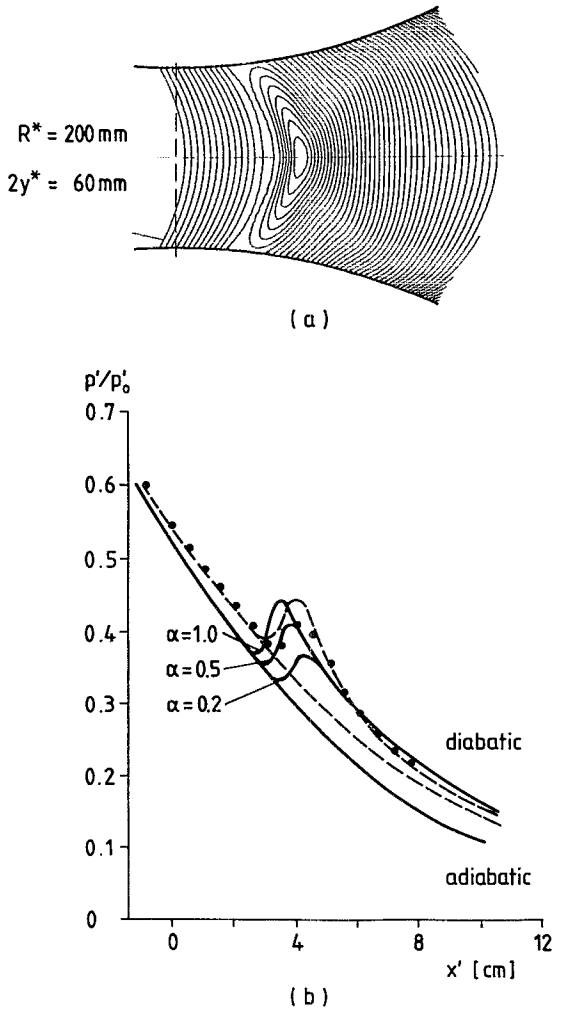

FIG. 6. (a) The Mach number ($M>1$) contours from the numerical 2-D finite volume simulation of Schnerr and Dohrmann (Ref. 28) in nozzle 2 under the atmospheric supply conditions $\varphi_0=36.6\%$, $\omega_0=8.3$ g/kg, $T_0'=300.3$ K (the increment between any two successive contours is $\Delta M=0.02$). (b) Distribution of the pressure along the axis of nozzle 2 under the atmospheric supply conditions $\varphi_0=36.6\%$, $\omega_0=8.3$ g/kg, and $T_0'=300.3$ K. ●, static pressure measurements in experiments conducted by Schnerr (Ref. 31), --- numerical 2-D finite volume simulation in the ice model with $\alpha=0.2$ by Schnerr and Dohrmann (Ref. 28) ($T_s'=281.0$ K, $T_k'=229.8$ K, $\Delta T_{ad}'\equiv T_s'-T_k'=51.2$ K, $M_k=1.238$, $J_{max}'=0.14\times10^{25}$ m^{-3} sec^{-1}). ——, 1-D asymptotic solution in the ice model with different values of α (in particular for $\alpha=0.2$, $T_s'=281.0$ K, $T_k'=223.4$ K, $\Delta T_{ad}'\equiv T_s'-T_k'=57.6$ K, $M_k=1.31$, $J_{max}'=0.97\times10^{25}$ m^{-3} sec^{-1}, $K=0.7987\times10^{-2}$, $\lambda=1190.4$).

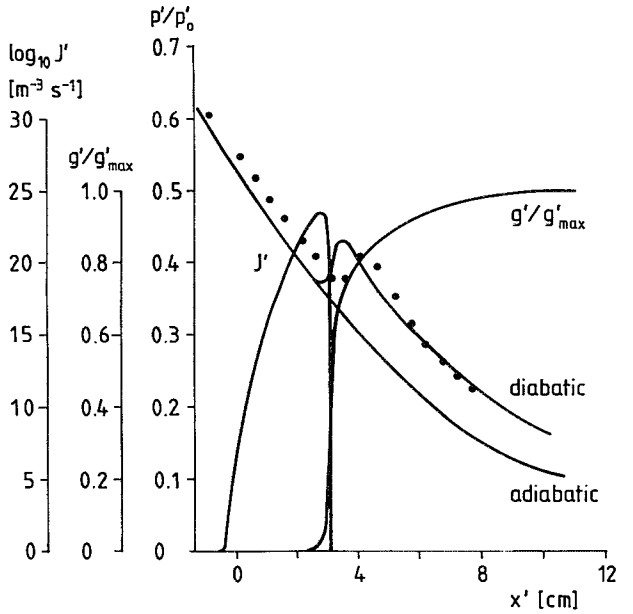

FIG. 7. Distribution of the pressure, the nucleation rate, and the condensate mass fraction along the axis of nozzle 2 under the atmospheric supply conditions $\varphi_0=36.6\%$, $\omega_0=8.3$ g/kg; $T_0'=300.3$ K. ●, static pressure measurements in experiments conducted by Schnerr (Ref. 31), ——, 1-D asymptotic solution in the liquid model where $\alpha=1$ for $x\geqslant x_k$ ($T_s'=280.7$ K, $T_k'=224.9$ K, $\Delta T_{ad}'\equiv T_s'-T_k'=55.8$ K, $M_k=1.295$, $J_{max}'=0.36\times10^{24}$ m^{-3} sec^{-1}, $K=0.7987\times10^{-2}$, $\lambda=14\,880.8$).

Knudsen droplet growth law. Only atmospheric supply conditions with relatively low initial relative humidity (30%–40%) are considered to ensure subcritical or smooth flows. Two models, LM and IM, describing the state of the condensed phase, respectively, as water drops or ice crystals are employed in identifying the essential thermodynamic properties such as latent heat, surface tension, and condensation coefficient (in the ice model the condensation coefficient is treated as a curve fitting parameter due to lack of reliable data). Two circular arc nozzles, one slender (nozzle 1) and the other effectively two dimensional (nozzle 2), are employed to exhibit the differences between the 1-D and 2-D flow fields with condensation, in particular, the effect of wall curvature on the 1-D condensing flow field.

The predictions of the 1-D asymptotic theory presented herein for moist air expansions under atmospheric supply conditions show good agreement with experimental data when the liquid model is employed in relatively slender nozzles. Although no certain knowledge of the state of the condensed phase (probably a mixture of water drops and ice crystals) is available in this case, the better agreement with experiments in the liquid model suggests that the dominant condensed phase most probably consists of water drops. Due to this nature of the condensed phase, no reliable estimate for the condensation coefficient of ice crystals could be deduced (a reliable estimate for α may perhaps be achieved in situations where the liquid model yields poorer agreement with experimental results). The predictions of the 1-D asymptotic theory are not in good agreement with the 2-D flow field structure of condensing nozzle flows when nozzles with significant wall curvatures are employed. In this case the improvement of the 1-D asymptotic theory to account for 2-D effects arising from wall curvature is essential.

ACKNOWLEDGMENTS

The authors are grateful to Dr. U. Dohrmann for providing the 2-D finite volume computations shown in Figs. 3 and 6.

One of the authors (C.F.D.) acknowledges the support by the Alexander von Humboldt Foundation during the performance of this work.

APPENDIX A: ASYMPTOTIC SOLUTION OF THE RATE EQUATION (16) IN THE INITIAL GROWTH (IGZ) AND FURTHER GROWTH (FGZ) ZONES

In both of these zones $dB/dx=O(1)$, and the asymptotic expressions for g and dg/dx follow from the solution of the rate equation by Laplace's method[10] in the double limit as $K\to 0$ and $\lambda\to\infty$:

$$g(x)\sim\Sigma(x)A(x)K^4\left(\frac{dB}{dx}\right)^{-4}\exp[-K^{-1}B(x)]\times\left[6\lambda^3\Omega^3(x)-6\lambda^2\Omega^2(x)\left(\frac{r^*(x)(dB/dx)}{K}\right)+3\lambda\Omega(x)\left(\frac{r^*(x)(dB/dx)}{K}\right)^2-\left(\frac{r^*(x)(dB/dx)}{K}\right)^3\right] \tag{A1}$$

and

$$\frac{dg}{dx}\sim-\Sigma(x)A(x)K^3\left(\frac{dB}{dx}\right)^{-3}\exp[-K^{-1}B(x)]\times\left[6\lambda^3\Omega^3(x)-6\lambda^2\Omega^2(x)\left(\frac{r^*(x)(dB/dx)}{K}\right)+3\lambda\Omega(x)\left(\frac{r^*(x)(dB/dx)}{K}\right)^2-\left(\frac{r^*(x)(dB/dx)}{K}\right)^3\right], \tag{A2}$$

where

$$\frac{dB}{dx}=\frac{\partial\tilde{B}}{\partial g}\frac{dg}{dx}+\frac{\partial\tilde{B}}{\partial x}. \tag{A3}$$

The above Eqs. (A1)–(A3) form a transcendental system for $g(x)$ and dg/dx and are solved iteratively, starting from the frozen ($g\equiv 0$) solution. In particular, the expressions for $g(x)$ and dg/dx in IGZ can be simplified[9,10] from Eqs. (A1) and (A2) in the limit as

$$B(x)\to B_f(x)\equiv\tilde{B}(0,x),\qquad \Sigma(x)\to\Sigma_f(x)\equiv\tilde{\Sigma}(0,x),\quad\text{etc.} \tag{A4}$$

It should also be mentioned that in the limit as $r^*\to 0$ Eqs. (A1)–(A3) reduce to the solution of FGZ (and together with the frozen limit to the solution of IGZ) given in Clarke and Delale.[10]

APPENDIX B: ASYMPTOTIC SOLUTION OF THE RATE EQUATION (16) IN THE RAPID GROWTH (RGZ) AND ONSET (OZ) ZONES

In these zones dB/dx diminishes to $O(K^{1/2})$ as $K\to 0$ by definition. From the solution of the rate equation (16) by Laplace's method,[10] after cumbersome manipulations it can be shown that the asymptotic expressions for g, dg/dx, and d^2g/dx^2 are of the form

$$g(x)\sim\Sigma(x)A(x)[2\beta(x)]^{-2}\exp[-K^{-1}B(x)]\exp\left(\frac{\gamma^2(x)}{8\beta(x)}\right)\left[6\lambda^3\Omega^3(x)D_{-4}\left(\frac{\gamma(x)}{\sqrt{2\beta(x)}}\right)+6\lambda^2\Omega^2(x)[r^*(x)\sqrt{2\beta(x)}]D_{-3}\left(\frac{\gamma(x)}{\sqrt{2\beta(x)}}\right)+3\lambda\Omega(x)[r^*(x)\sqrt{2\beta(x)}]^2D_{-2}\left(\frac{\gamma(x)}{\sqrt{2\beta(x)}}\right)+[r^*(x)\sqrt{2\beta(x)}]^3D_{-1}\left(\frac{\gamma(x)}{\sqrt{2\beta(x)}}\right)\right], \tag{B1}$$

$$\frac{dg}{dx}\sim\Sigma(x)A(x)[2\beta(x)]^{-3/2}\exp[-K^{-1}B(x)]\exp\left(\frac{\gamma^2(x)}{8\beta(x)}\right)\left[6\lambda^3\Omega^3(x)D_{-3}\left(\frac{\gamma(x)}{\sqrt{2\beta(x)}}\right)+6\lambda^2\Omega^2(x)[r^*(x)\sqrt{2\beta(x)}]D_{-2}\left(\frac{\gamma(x)}{\sqrt{2\beta(x)}}\right)+3\lambda\Omega(x)[r^*(x)\sqrt{2\beta(x)}]^2D_{-1}\left(\frac{\gamma(x)}{\sqrt{2\beta(x)}}\right)+[r^*(x)\sqrt{2\beta(x)}]^3\exp\left(-\frac{\gamma^2(x)}{8\beta(x)}\right)\right], \tag{B2}$$

and

$$\frac{d^2g}{dx^2}\sim\frac{1}{\Omega(x)}\frac{d\Omega}{dx}\frac{dg}{dx}+\Sigma(x)A(x)[2\beta(x)]^{-1}\exp[-K^{-1}B(x)]\exp\left(\frac{\gamma^2(x)}{8\beta(x)}\right)\left[6\lambda^3\Omega^3(x)D_{-2}\left(\frac{\gamma(x)}{\sqrt{2\beta(x)}}\right)+6\lambda^2\Omega^2(x)[r^*(x)\sqrt{2\beta(x)}]D_{-1}\left(\frac{\gamma(x)}{\sqrt{2\beta(x)}}\right)+3\lambda\Omega(x)[r^*(x)\sqrt{2\beta(x)}]^2\exp\left(-\frac{\gamma^2(x)}{8\beta(x)}\right)\right.$$

$$+[r^*(x)\sqrt{2\beta(x)}]^3\exp\left(-\frac{\gamma^2(x)}{8\beta(x)}\right)$$
$$\times\frac{\{[3/r^*(x)](dr^*/dx)+[1/\Sigma(x)](d\Sigma/dx)+[1/A(x)](dA/dx)+\gamma(x)-[1/\Omega(x)](d\Omega/dx)\}}{\sqrt{2\beta(x)}}\Bigg], \tag{B3}$$

where

$$\gamma(x)\equiv -K^{-1}\left(\frac{dB}{dx}\right)\geqslant 0, \tag{B4}$$

$$\beta(x)\equiv\frac{1}{2}K^{-1}\left(\frac{d^2B}{dx^2}\right)>0, \tag{B5}$$

with

$$\frac{dB}{dx}=\frac{\partial\tilde{B}}{\partial g}\frac{dg}{dx}+\frac{\partial\tilde{B}}{\partial x}, \tag{B6}$$

$$\frac{d^2B}{dx^2}=\frac{\partial\tilde{B}}{\partial g}\frac{d^2g}{dx^2}+\frac{\partial^2\tilde{B}}{\partial g^2}\left(\frac{dg}{dx}\right)^2+2\frac{\partial^2\tilde{B}}{\partial g\,\partial x}\frac{dg}{dx}+\frac{\partial^2\tilde{B}}{\partial x^2}, \tag{B7}$$

$$\frac{dr^*}{dx}=\frac{\partial\tilde{r}^*}{\partial g}\frac{dg}{dx}+\frac{\partial\tilde{r}^*}{\partial x}, \tag{B8}$$

$$\frac{d\Omega}{dx}=\frac{\partial\tilde{\Omega}}{\partial g}\frac{dg}{dx}+\frac{\partial\tilde{\Omega}}{\partial x}, \tag{B9}$$

$$\frac{d\Sigma}{dx}=\frac{\partial\tilde{\Sigma}}{\partial g}\frac{dg}{dx}+\frac{\partial\tilde{\Sigma}}{\partial x}, \tag{B10}$$

where $D_{-n}(x)$; $n=1,2,3,4$ denote Whittaker's parabolic cylinder function.[33,34] Equations (B1)–(B10) provide a complete transcendental solution for g, dg/dx, and d^2g/dx^2 in RGZ and OZ and are solved locally by an iterative scheme, starting with a nearby upstream solution. In particular, the solutions for g_l, $(dg/dx)_l$, and $(d^2g/dx^2)_l$ at the "relative onset point" (herein by subscript l we mean evaluated at $x=x_l$), follow in the limit as

$$\gamma\to\gamma_l\equiv 0,\quad \beta\to\beta_l\equiv\frac{1}{2}K^{-1}\left(\frac{d^2B}{dx^2}\right)_l,\quad \Sigma\to\Sigma_l,\ \text{etc.}, \tag{B11}$$

where the parabolic cylinder functions take the following values:

$$D_{-1}(0)=\sqrt{\frac{\pi}{2}},\quad D_{-2}(0)=1,$$
$$D_{-3}(0)=\frac{1}{2}\sqrt{\frac{\pi}{2}},\quad D_{-4}(0)=\frac{1}{3}. \tag{B12}$$

Furthermore, when $r^*\to 0$ and the first term of Eq. (B3) is neglected on order of magnitude estimates, we recover the solution for these zones given in Clarke and Delale.[10]

APPENDIX C: ASYMPTOTIC SOLUTION OF THE RATE EQUATION (16) IN THE NUCLEATION ZONE WITH GROWTH (NZ)

In this zone the asymptotic solution for g follows from the solution of the rate equation (16), where the relative onset point x_l (defined by the condition $\gamma_l=0$) acts as an interior minimum for Laplace's method.[10] Consequently, we have

$$g(\phi)\sim b_l[(r_l^*+a_l\phi)^3F_0(\phi)-3a_l(r_l^*+a_l\phi)^2F_1(\phi)$$
$$+3a_l^2(r_l^*+a_l\phi)F_2(\phi)-a_l^3F_3(\phi)], \tag{C1}$$

where

$$\phi\equiv K^{-1/2}\left(\frac{1}{2}\frac{d^2B}{dx^2}\right)_l^{1/2}(x-x_l)=\sqrt{\beta_l}(x-x_l)\geqslant 0, \tag{C2}$$

$$a_l\equiv\lambda\Omega_l\beta_l^{-1/2}, \tag{C3}$$

$$b_l\equiv\Sigma_lA_l\beta_l^{-1/2}\exp(-K^{-1}B_l), \tag{C4}$$

and

$$F_r(\phi)\equiv\int_{-\infty}^{\phi}\zeta^re^{-\zeta^2}\,d\zeta,\quad r=0,1,2,3. \tag{C5}$$

It should be mentioned that the functions $F_r(\phi)$, $r=0,1,2,3$ given by Eq. (C5) can be related to the elementary error function. When $\phi=0$, we precisely recover the expression for g_l obtained in the limit $\gamma\to\gamma_l\equiv 0$ in Appendix B. On the other hand, as $\phi\to\infty$, we have

$$g(\phi)\sim\sqrt{\pi}b_la_l^3\left[\phi^3+3\left(\frac{r_l^*}{a_l}\right)\phi^2+3\left[\frac{1}{2}+\left(\frac{r_l^*}{a_l}\right)^2\right]\phi+\left(\frac{r_l^*}{a_l}\right)^3\right.$$
$$\left.+\frac{3}{2}\left(\frac{r_l^*}{a_l}\right)\right], \tag{C6}$$

corresponding to a cubic growth law. We should also mention that in the limit as $r_l^*\to 0$, we recover in NZ the same asymptotic expression for g given in Clarke and Delale.[10]

APPENDIX D: ASYMPTOTIC SOLUTION OF THE RATE EQUATION (16) IN THE DROPLET GROWTH ZONE (DGZ)

The cubic growth law of Eq. (C6) cannot persist over the total length of this zone, since thermodynamic equilibrium is reached in this zone. Using Laplace's method for an interior minimum,[10] the solution of the rate equation (16) in this zone can be cast into the asymptotic form

$$g(x;K) \sim \sqrt{\pi} b_l \lambda^3 \Omega_l^3 \left([R(x;K)]^3 + 3\frac{r_l^*}{\lambda\Omega_l}[R(x;K)]^2 + 3\frac{(r_l^{*2}+\frac{1}{2}a_l^2)}{\lambda^2\Omega_l^2} R(x;K) + \frac{(r_l^{*3}+\frac{3}{2}a_l^2 r_l^*)}{\lambda^3\Omega_l^3} \right), \quad \text{(D1)}$$

where

$$R(x;K) \equiv \int_{x_l}^{x} \frac{\Omega(\xi;K)}{\Omega_l} d\xi. \quad \text{(D2)}$$

Introducing the scaling variables,

$$\chi \equiv \Lambda K^{-1/3}(x - x_l), \quad \text{(D3)}$$

$$\bar{R} \equiv \Lambda K^{-1/3} R(x;K), \quad \text{(D4)}$$

for $x > x_l$, with

$$\Lambda \equiv \lambda \Omega_l (\sqrt{\pi} K b_l)^{1/3}, \quad \text{(D5)}$$

we obtain

$$g \sim \bar{R}^3 + 3r_l^* (\sqrt{\pi} b_l)^{1/3} \bar{R}^2 + 3(r_l^{*2} + \tfrac{1}{2}a_l^2)(\sqrt{\pi} b_l)^{2/3} \bar{R} + (r_l^{*3} + \tfrac{3}{2}a_l^2 r_l^*)(\sqrt{\pi} b_l), \quad \text{(D6)}$$

where $\bar{R}$ is determined from the relaxation rate equation

$$\frac{d\bar{R}}{d\chi} = \bar{\Omega}, \quad \text{(D7)}$$

with $\bar{R} = 0$ at $\chi = 0$ and $\bar{\Omega} \equiv \Omega/\Omega_l$. It is important to note that the scaling variables introduced in Eqs. (D3)–(D4), which can be arrived at from order of magnitude estimates now by ordering the double limit as $K \to 0$ and $\lambda \to \infty$ in the same way as given in Clarke and Delale,[10] namely

$$\lambda^3 = O[K^{-3/2} \exp(K^{-1} B_l)], \quad \text{as } K \to 0, \quad \text{(D8)}$$

have no effect whatsoever on the solution of the rate equation and local flow field, except for being convenient variables for numerical computations. The nonlinear droplet growth relaxation equation (D7) is of the same form as nonequilibrium internal mode excitation or chemical reaction with flow and tends to saturated states in local thermodynamic equilibrium so that $\bar{\Omega} \to 0$ as $\chi \to \infty$. Furthermore, in the limit as $r_l^* \to 0$, the asymptotic solution of the rate equation (16) presented herein reduces to the corresponding one in DGZ given by Clarke and Delale.[10]

[1] L. Prandtl, "Allgemeine überlegungen die strömung zusammendrückbarer flüssigkeiten," Reale Acc. Italia, Roma **XIV**, 167 (1936).
[2] K. Oswatitsch, "Kondensationserscheinungen in überschalldüsen," Z. Angew. Math. Mech. **22**, 1 (1942).
[3] P. P. Wegener and L. M. Mack, "Condensation in supersonic and hypersonic wind tunnels," in *Advances in Applied Mechanics* (Academic, New York, 1958), Vol. V, p. 307.
[4] H. G. Stever, "Condensation in high speed flows," in *Fundamentals of Gas Dynamics, High Speed Aerodynamics and Jet Propulsion* (Princeton University Press, Princeton, NJ, 1958), p. 526.
[5] P. P. Wegener, "Gasdynamics of expansion flows with condensation and homogeneous nucleation of water vapor," in *Nonequilibrium Flows*, edited by P. P. Wegener (Marcel Dekker, New York, 1969), Part 1.
[6] P. G. Hill, "Condensation of water vapor during supersonic expansion in nozzles," J. Fluid Mech. **25**, 593 (1966).
[7] D. Barschdorff, "Verlauf der zustandsgrössen und gasdynamischen zusammenhänge bei der spontanen kondensation reinen wasserdampfes in lavaldüsen," Forsch. Ing. **37**, 146 (1971).
[8] G. Gyarmathy, "Théorie de le condensation en cours de détente dans les turbines a vapeur," Rev. Fr. Mech. **57**, 35 (1976).
[9] P. A. Blythe and C. J. Shih, "Condensation shocks in nozzle flows," J. Fluid Mech. **76**, 593 (1976).
[10] J. H. Clarke and C. F. Delale, "Nozzle flows with nonequilibrium condensation," Phys. Fluids **29**, 1398 (1986).
[11] C. F. Delale, "Two dimensional supersonic expansion flows on walls with nonequilibrium condensation," Ph.D. thesis, Brown University, 1983.
[12] A. Erdelyi, *Asymptotic Expansions* (Dover, New York, 1956).
[13] G. Carrier, M. Krook, and C. Pearson, *Functions of a Complex Variable: Theory and Technique* (McGraw-Hill, New York, 1966).
[14] L. Sirovich, *Techniques of Asymptotic Analysis* (Springer-Verlag, New York, 1971).
[15] M. Volmer and A. Weber, "Keimbildung in übersättigten gebilden," Z. Phys. Chem. A **119**, 277 (1926).
[16] L. Farkas, "Keimbildungsgeschwindigkeit in übersättigten dämpfen," Z. Phys. Chem. A **125**, 236 (1927).
[17] R. Becker and W. Döring, "Kinetische behandlung der keimbildung in übersättigten dämpfen," Ann. Phys. **24**, 719 (1935).
[18] M. Volmer, *Kinetik der Phasenbildung* (Steinkopff, Dresden, 1939).
[19] Y. B. Z'eldovich, "Theory of formation of a new phase: Cavitation," J. Exp. Theor. Phys. USSR **12**, 525 (1942).
[20] J. Frenkel, *Kinetic Theory of Liquids* (Oxford University Press, Oxford, 1946).
[21] J. Lothe and G. M. Pound, "Reconsiderations of nucleation theory," J. Chem. Phys. **36**, 2080 (1962).
[22] W. G. Courtney, "Nonsteady state nucleation," J. Chem. Phys. **36**, 2009 (1962); "Kinetics of condensation of water vapor," *ibid.* **36**, 2018 (1962).
[23] A. C. Zettlemoyer, *Nucleation* (Marcel Dekker, New York, 1969).
[24] V. P. Skripov, *Metastable Liquids* (Wiley, New York, 1969).
[25] J. Feder, K. C. Russell, J. Lothe, and G. M. Pound, "Homogeneous nucleation and growth of droplets in vapours," Adv. Phys. **15**, 1 (1966).
[26] A. Dillmann and G. E. A. Meier, "A refined droplet approach to the problem of homogeneous nucleation from the vapor phase," J. Chem. Phys. **94**, 3872 (1991).
[27] D. Sonntag and D. Heinze, *Sättigungsdampfdruck-und Sätigungsdampfdichtetafeln für Wasser and Eis* (VEB Deutscher-Verlag, Leipzig, 1982).
[28] G. Schnerr and U. Dohrmann, "Theoretical and experimental investigation of 2-D diabatic transonic and supersonic flow fields," in *Proceedings of the IUTAM Symposium Transsonicum III*, edited by J. Zierep and H. Oertel (Springer-Verlag, Berlin, 1989), p. 131.
[29] F. Peters and B. Paikert, "Nucleation and growth rates of homogeneously condensing water vapor in argon from shock tube experiments," Exp. Fluids **7**, 521 (1989).
[30] U. Grigull, *Properties of Water and Steam in SI-Units* (Springer-Verlag, Berlin, 1979).
[31] G. Schnerr, "2-D transonic flow with energy supply by homogeneous condensation: Onset condition and 2-D structure of steady Laval nozzle flow," Exp. Fluids **7**, 145 (1989).
[32] J. H. Clarke and C. F. Delale, "Expansion flows on walls with nonequilibrium condensation," Q. Appl. Math. **XLVI**, 121 (1988).
[33] M. Abramowitz and A. Stegun, *Handbook of Mathematical Functions* (Dover, New York, 1965).
[34] I. S. Gradshteyn and I. M. Ryzhik, *Tables of Integrals, Series and Products* (Academic, New York, 1980).